Applied Catalysis B: Environmental 237 (2018) 563–573

Contents lists available at ScienceDirect

Applied Catalysis B: Environmental

journal homepage: www.elsevier.com/locate/apcatb

High efficient photocatalytic hydrogen evolution from formaldehyde over sensitized Ag@Ag-Pd alloy catalyst under visible light irradiation

Hongxia Liu[a,b,c], Meng Wang[a,b,c], Xuqiang Zhang[a], Jiantai Ma[c], Gongxuan Lu[a,*]

[a] State key Laboratory for Oxo Synthesis and Selective Oxidation, Lanzhou Institute of Chemical Physics, Chinese Academy of Science, Lanzhou 730000, China
[b] University of Chinese Academy of Science, Beijing 100049, China
[c] College of Chemistry and Chemical Engineering, Lanzhou University, Lanzhou, 730000, China

ARTICLE INFO

Keywords:
Photocatalytic hydrogen generation
Formaldehyde
Visible light irradiation
Sensitized Ag@Ag-Pd core-shell nanocapsule catalyst
Surface active sites modulation

ABSTRACT

The development of an active but cheaper catalyst is critical for efficient photocatalytic hydrogen from renewable source. In this study, we develop a high active catalyst for hydrogen evolution from formaldehyde *via* alloying of Pd with Ag and sensitization with a dye eosin Y (EY). The XRD, XPS, TEM and HRTEM characterizations indicate that the catalyst exhibits a core-shell structure (Ag core and Ag-Pd shell). Alloying Pd with Ag not only provides more efficient catalytic sites than single component Pd catalyst, but greatly promotes the efficient electron transfer and prolongs the lifetime of photogenerated electrons, enhances the charge separation efficiency and the photocatalytic hydrogen evolution activity significantly. The catalyst activity for hydrogen is highly dependent on the adsorption energies of HCHO and H_2O molecules on metal surface of the alloy catalyst. Our results disclose a new route to high efficient catalyst development for solar hydrogen generation from formaldehyde.

1. Introduction

The rapid depletion of fossil fuels (oil, gas, and coal) and related environmental pollution have been pushing forward the extensive search for efficient, clean and renewable energy resources [1–17]. Hydrogen is considered as an ideal renewable energy carrier for replacement of fossil fuels due to its high energy density and the environment friendly emission characteristics in its usage. Many efforts have been devoted to find the new routes for hydrogen generation from renewable sources, such as biomass, *via* steam reforming or gasification [18–36]. During the gasification of biomass, large amount of formaldehyde is produced, therefore catalytic conversion formaldehyde to hydrogen can be an efficient way to generate hydrogen [37]. Although formaldehyde can be thermal catalytic converted into hydrogen over noble metal loaded catalysts [38–45], photocatalytic conversion formaldehyde into hydrogen can be operated under more mild conditions, and the obtained technique can be also used in other environmental concerned issues, such as toxic organic remediation [46].

It is known that loaded Pd, Pt nanoparticles can catalyze formaldehyde into hydrogen under light irradiation, for example, Pt/TiO_2 [47], due to their high activity and low overpotential for proton reduction, but high cost of noble metals precludes their widespread utilization [48,49]. Alloying Pt or Pd with the second metal can not only reduce the consumption of noble metal, but also enhance the activity of the catalyst because the dispersion of noble metal can be improved. Other effects of component alloying have been reported as well, such as the lattice mismatch in crystal and ligand effect [50,51]. For instance, the oxygen reduction activity of Pt alloys supported on carbon black was enhanced by alloying and lattice mismatch [52], and the activity and selectivity for hydrogenation and hydrogen evolution of Pd-based alloy catalysts could be promoted by electronic ligand effect [53–59].

Among the second coordination metals, Ag is a cheaper and more abundant element than Pt, Pd, Au and other noble elements [55,60]. In this paper, a new strategy of photocatalyst design *via* Ag alloying of Pd for hydrogen generation from formaldehyde under visible light irradiation has been developed. By variation of the Ag-Pd ratio in alloy, a new and high active Ag-Pd alloy catalyst for hydrogen generation has been developed. The $Ag@Ag_1Pd_1$ catalyst showed the highest activity among all the catalyst samples. Over this $Ag@Ag_1Pd_1$ photocatalyst, the more efficient photogenerated electron transfer and proton reduction have been achieved by modification of catalytic active sites. Our results disclose a new route to develop efficient alloy catalyst for hydrogen generation from formaldehyde.

* Corresponding author.
E-mail address: gxlu@lzb.ac.cn (G. Lu).

https://doi.org/10.1016/j.apcatb.2018.06.028
Received 7 April 2018; Received in revised form 7 June 2018; Accepted 9 June 2018
Available online 15 June 2018

2. Experimental methods

2.1. Materials

Silver nitrate ($AgNO_3$, Chengdu Kelong Chemical Regent Co., Ltd, AR, ≥99.8%), polyvinylpyrrolidone PVP (PVP, Aladdin, Mw = 58000), ethylene glycol ($(HCHOH)_2$, Xilong Chemical Co., Ltd, AR, ≥99.5%), ferric chloride hexahydrate ($FeCl_3{\cdot}6H_2O$, Tianjin Kemiou Chemical Reagent Co., Ltd, AR, ≥99.0%), palladium chloride ($PdCl_2$, Tianjin Kemiou Chemical Reagent Co., Ltd, AR, ≥59%), sodium chloride (NaCl, Xilong Chemical Co., Ltd, AR, > 99.5%), sodium hydroxide (NaOH, Xilong Chemical Co., Ltd., AR, > 96%), formaldehyde (HCHO, Xilong Chemical Co., Ltd., AR, 37%–40%) were purchased and used without further purification. Deionized water was used in the synthesis and reaction.

2.2. Catalysts preparation

Catalysts were prepared as following. First, the Ag nanowire was synthesized by reducing silver nitrate in ethylene glycol (EG) according to the reference [61]. Under vigorous stirring, 1 g PVP power was dispersed in 50 ml EG solution, then 1 g $AgNO_3$ was dissolved in little amount of EG solution and 14 g $FeCl_3$ (600 μmol/L) was added to get the mixture solution, the obtained solution was heated to 130 °C and was kept for 5 h. After cooled mixture to room temperature, the products were collected and washed with acetone repeatedly to remove EG.

The hollow Ag-Pd alloy was synthesized according to literature [62]. The obtained Ag nanowire was dispersed in saturated sodium chloride solution. The $PdCl_2$ dispersions was prepared by dissolving calculated amount of $PdCl_2$ powder in the deionized water. The $PdCl_2$ solution were added to the Ag nanowire water mixture drop by drop under stirring at room temperature, then the product was collected and washed with water repeatedly to remove chloride ions (see Scheme 1).

The hollow Pd nanotube was synthesized according to literature [63]. The mixture containing the as-synthesized Ag nanowires (10 mg) was added to saturated NaCl aqueous solution. Then the $PdCl_2$ solution (0.02 M) was added to the Ag nanowires mixture slowly under the room temperature. The obtained samples were washed with deionized water and ethanol to remove AgCl and NaCl. Finally, H_2O_2 solution was used to remove the remnant Ag.

2.3. Catalytic property measurement

Photocatalytic experiments were performed at room temperature in a sealed Pyrex flask (195 mL) with a flat window and a silicone rubber septum for sampling. The details of the experiment procedure were as follows. 10 mg catalyst and 35 mg Eosin Y (EY) was added to 100 ml NaOH (pH = 14) solution in the Pyrex flask and the mixture was degassed by bubbling Ar gas for 30 min to exclude the air. After degassing by Ar, a calculated amount of formaldehyde was added to the mixture. The light source was a 300 W Xenon lamp with a 420 nm cut-off filter. The hydrogen evolution rate was measured by detection of the evolved hydrogen using a gas chromatography (Agilent 6820, TCD, 13 × column, Ar carrier). The blank test was performed in a similar procedure except no catalyst or under dark. The recycling test of catalyst was carried out as follows. Typically, after the reaction of the first run, the catalyst was removed from mixture by centrifugation and was added to the reactor again. New run of reaction was carried out according to the procedure mentioned above.

2.4. Isotope tracer experiments

In order to identify the hydrogen formation mechanism, the isotopes tracer experiments were performed using D_2O instead of H_2O. The gas mixture in container was measured by GC–MS (Aglient, 5975c, Triple-Axis Detector) or a Quadrupole Mass Spectrometer (LC-D200 M).

2.5. Characterizations

Transmission electron microscopy (TEM) and high-resolution transmission electron microscopy (HRTEM) analysis were performed on a Tecnai-G2-F30 field emission transmission electron microscope with a 300 kV accelerating voltage. X-ray diffraction (XRD) patterns of catalysts were obtained on a Rigaku B/Max-RB X-ray diffractometer with a nickel-filtrated Cu Kα radiation operated at 40 kV and 40 mA. X-ray photoelectron spectroscopy (XPS) measurements were conducted on a VG Scientific ESCALAB 210-XPS photoelectron spectrometer with a Mg

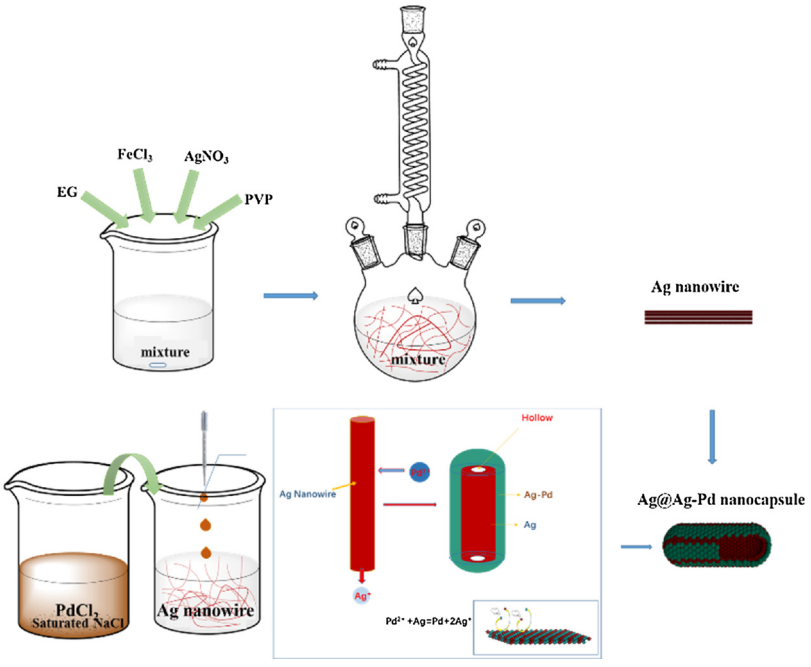

Scheme 1. The preparation process of the catalyst.

Kα X-ray resource. The UV–vis absorption spectra were acquired with a UV 2600PC, Japan spectrophotometer

2.6. Photoelectrochemical performance

All the electrochemical measurements were measured on an electrochemical analyzer (CHI660E) in a homemade standard three-electrode quartz cell consisting of an organic glass enclosure with a quartz window and a 1.2 cm diameter opening opposite the window to the work electrode was clamped. The working electrode was prepared by drop-coating sample suspensions directly onto the pre-cleaned indium tin oxide glass (ITO glass) surface. Platinum plate was used as the counter electrode and a saturated calomel electrode (SCE) as the reference electrode. The electrolyte was 0.5 M aqueous H_2SO_4 solution without any additives. The visible light irradiation source was a 300 W Xe arc lamp system equipped with a 420 nm cut-off filter. The surface area of the working electrode exposed to the electrolyte was about 0.95 cm^2.

3. Results and discussion

3.1. XRD analysis

The XRD patterns of synthesized Ag@Ag-Pd nanocapsule catalysts with different Ag/Pd ratios are presented in Fig. 1a. The typical peaks of Ag (111), (200), (220), (311) and (222) in catalysts located at 38.12°, 44.30°, 64.46°, 77.41° and 81.56° could be observed respectively (JCPDS-89-3722). The corresponding peaks of Pd (111), (200), (220), (311) and (222) in catalysts located at 39.06°, 45.41°, 66.17°, 79.61° and 83.92° were also observed (JCPDS-87-0637). XRD patterns in Fig. 1b present that the fine characteristics of (111) facet in the Ag@Ag-Pd nanocapsule catalysts with different Ag/Pd ratio. The XRD results indicate that Ag and Pd are in alloy state in $Ag@Ag_2Pd_1$, $Ag@Ag_1Pd_1$ and $Ag@Ag_1Pd_2$ catalysts [64].

3.2. XPS analysis

The Ag-Pd alloy catalysts with different Ag-Pd ratio were also analyzed by XPS and the chemical states of each element in catalysts were investigated (see Fig. 2). The ratio of the Ag and Pd peak areas in XPS confirmed the composition of Ag@Ag-Pd catalysts as Ag_2Pd_1, Ag_1Pd_1 and Ag_1Pd_1, respectively [65,66]. As the results shown in Fig. 2a, the Ag 3d in $Ag@Ag_1Pd_1$ catalyst shifted about 0.7 eV to negative side compared with metallic Ag [58,67], from 367.66 and 373.68 eV to 368.35 and 374.43 eV. In Fig. 2b, two peaks at 335.68 and 341.02 eV could be assigned to Pd $3d_{3/2}$ and Pd $3d_{5/2}$ of metallic Pd [59,68], and peaks at 334.75 and 340.05 eV could assigned to the Pd of Pd $3d_{3/2}$ and Pd $3d_{5/2}$ in $Ag@Ag_1Pd_1$ catalyst [69]. The XPS results indicate that Ag and Pd are in metallic state in the catalysts. The binding energy shifts of Ag and Pd reflect the strong interaction of Ag and Pd in catalyst due to the d orbital interaction [70].

3.3. Morphology analysis

The fine structures and morphology characteristics of Ag-Pd catalysts were further characterized by the transmission electron microscopy (TEM) and high-resolution transmission electron microscopy (HRTEM). The TEM images and HRTEM images of Ag-Pd catalysts were shown in Fig. 3. From the TEM images in Fig. 3a, c, e, the as-prepared catalyst exhibited a nanocapsule morphology. When the ratio of Pd-Ag increased, the nanocapsule gradually changed into a hollow structure. The HRTEM images of the Ag-Pd nanocapsule with different Pd-Ag ratio were also shown in Fig. 3. The lattice spacing of 0.232 nm in Fig. 3b could be assigned to the (111) face-centered cubic (fcc) Ag_2Pd_1, the lattice spacing of 0.231 nm and 0.230 nm in Fig. 3d and 3f correspond to the (111) Ag_1Pd_1 and Ag_1Pd_2 alloy. These results indicate the lattice strain effect in the alloy formation in galvanic replacement process, *i.e.*, Pd replacing Ag to form Ag-Pd alloy nanocapsule [71,72]. Pd^{2+} ions transfer onto the surfaces of the Ag, and oxidize Ag to Ag^+, while Pd^{2+} is reduced to metallic Pd, forming a thin layer of Ag-Pd alloy shell with hollow structures.

The HRTEM images of the Ag@Ag-Pd nanocapsule are shown in Fig. 4(a–d). The lattice spacing of 0.235 nm (see Fig. 4b) could be assigned to the (111) fcc Ag, and the lattice spacing of 0.231 nm (see Fig. 4d) could be assigned to (111) fcc Ag_1Pd_1 in $Ag@Ag_1Pd_1$ catalyst. These results confirmed the Ag-Pd alloy nanocapsule catalyst was in core-shell structure, with Ag core and Ag-Pd alloy shell (Ag@Ag-Pd nanocapsule). HAADF-STEM (high-angle annular dark field scanning transmission electron microscopy, (see Fig. 4e) images and elemental mapping images of the catalyst show that the element Pd and Ag distribute uniformly on the surface of the catalyst.

3.4. UV-Vis analysis

Fig. 5a shows the UV–Vis spectra of Ag nanowire and Pd nanotube. The peak centered at 410 nm is the typical surface plasma resonance

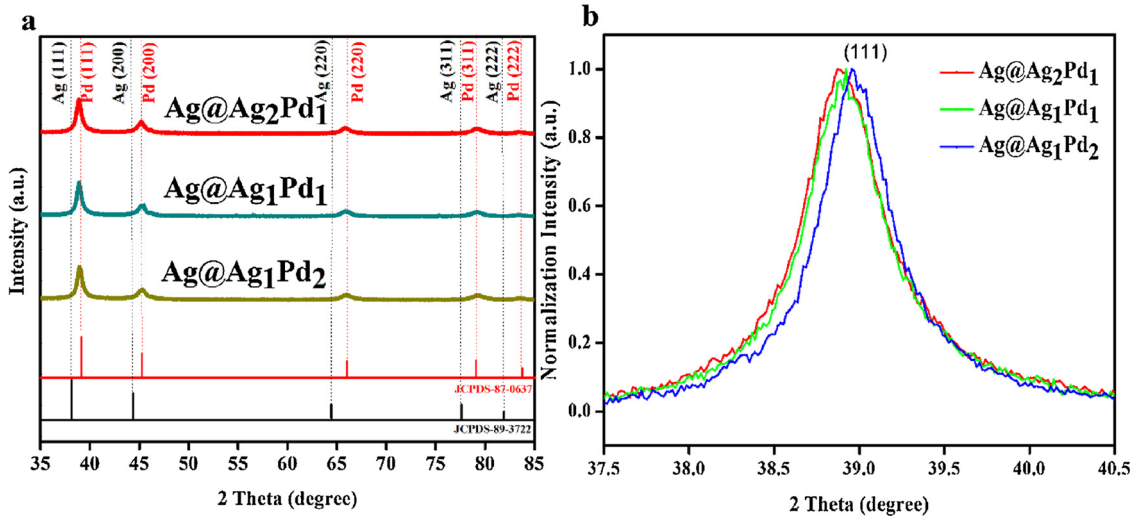

Fig. 1. (a) XRD patterns of Ag@Ag-Pd catalysts with different Ag/Pd ratio. (b) The normalized (111) XRD patterns of the Ag@Ag-Pd catalysts with different Ag/Pd ratio.

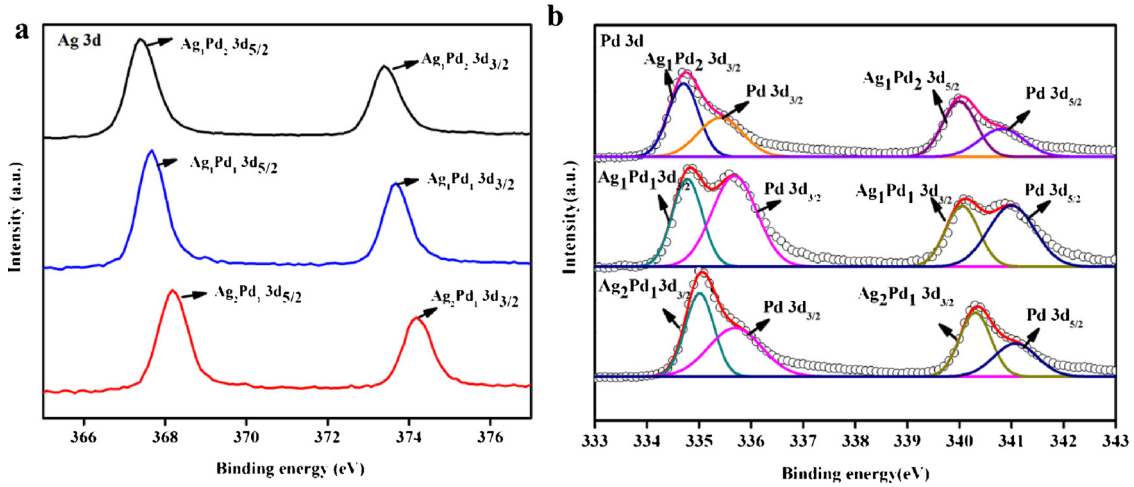

Fig. 2. XPS spectra of the Ag@Ag_2Pd_1, Ag@Ag_1Pd_1 and Ag@Ag_1Pd_2 catalysts. (a) Ag 3d of the Ag@Ag_2Pd_1, Ag@Ag_1Pd_1 and Ag@Ag_1Pd_2 catalysts; (b) Pd3d of the Ag@Ag_2Pd_1, Ag@Ag_1Pd_1 and Ag@Ag_1Pd_2catalysts.

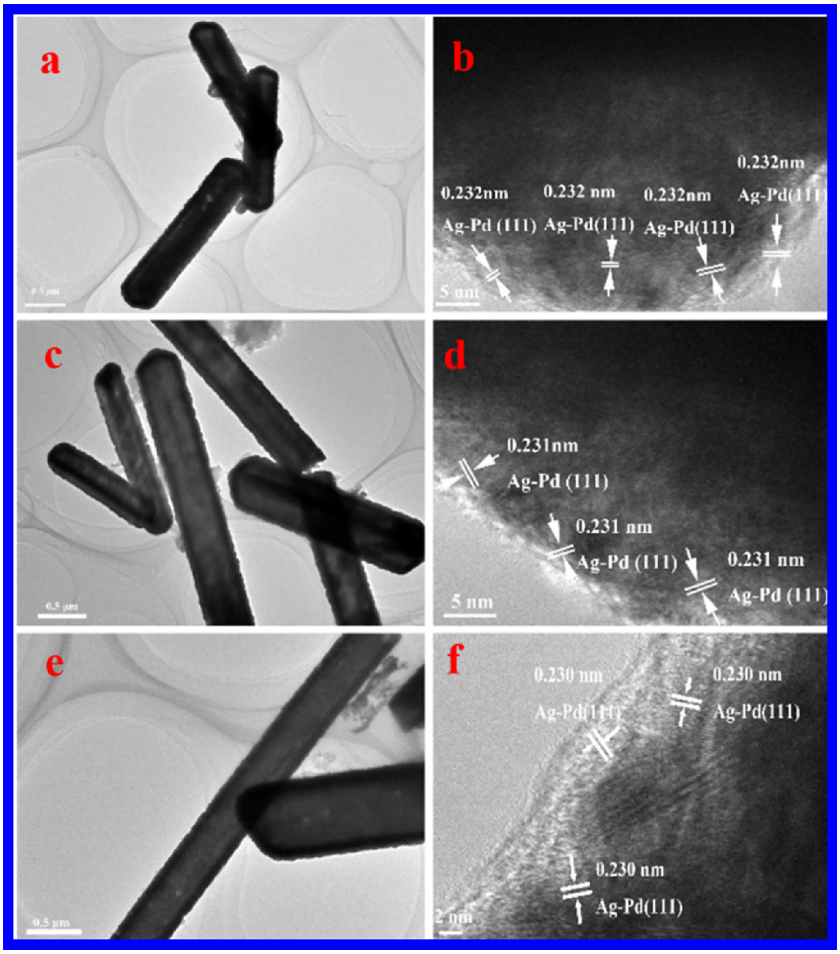

Fig. 3. The TEM and HRTEM images of Ag@Ag-Pd nanocapsule catalysts with different Ag/Pd ratio, (a) the TEM image of Ag@Ag_2Pd_1; (b) the HRTEM image of Ag@Ag_2Pd_1; (c) the TEM image of Ag@Ag_1Pd_1; (d) the HRTEM image of Ag@Ag_1Pd_1; (e) the TEM image of Ag@Ag_1Pd_2; (f) the HRTEM image of Ag@Ag_1Pd_2.

absorption of Ag. Pd nanoparticles does not give such kind of absorption. These results are similar to the previous reports [73,74]. The spectra of the Ag@Ag-Pd nanocapsule catalysts (Fig. 5b) with different Ag-Pd ratio show broad absorption tails from 400 to 800 nm, but do not show the characteristic peaks corresponding to the Ag nanoparticles, suggesting the formation of the Ag-Pd alloy [75], because there is peak centered at 410 nm for the physical mixture of Ag and Pd particles (see Fig. 5c) [76].

After dye sensitization with EY, catalysts show strong absorption centered at 518 nm (as shown in Fig. 6), which corresponds to the typical absorption of dye molecule. These results indicate that the sensitized Ag@Ag_1Pd_2, Ag@Ag_1Pd_1 and Ag@Ag_2Pd_1 catalysts can absorb visible light with wavelength longer than 440 nm, and the strongest absorption locate at 518 nm.

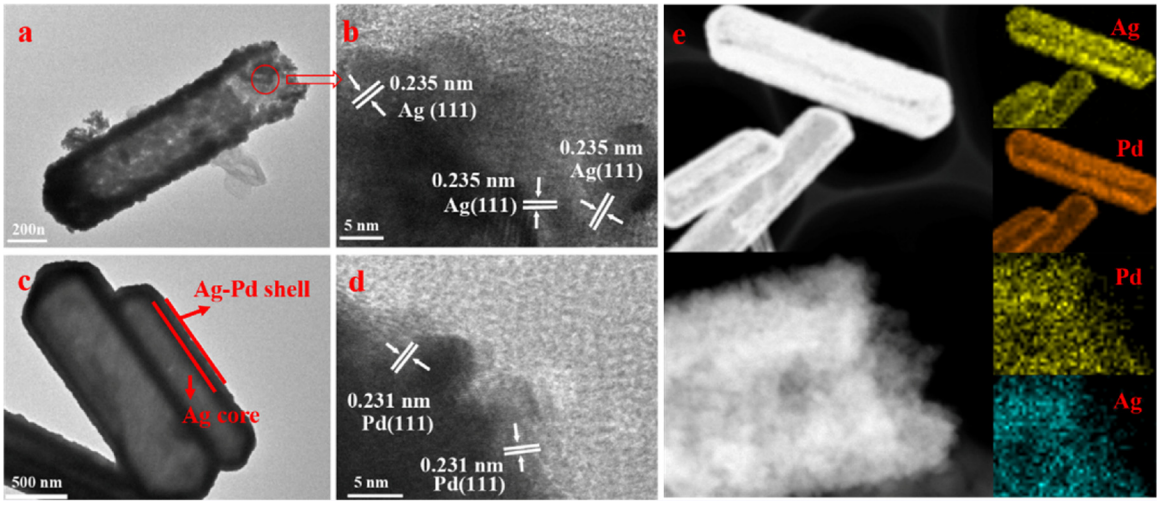

Fig. 4. The TEM and HRTEM images of Ag@Ag-Pd alloy catalysts; (a and c) TEM of as prepared $Ag@Ag_1Pd_1$ alloy catalyst; (b and d) HRTEM image of $Ag@Ag_1Pd_1$ catalyst; (e)HAADF-STEM (high-angle annular dark field scanning transmission electron microscopy) image and elemental mapping images of $Ag@Ag_1Pd_1$ catalyst.

3.5. Catalytic activity performance

The photocatalytic performance of photocatalysts was studied under visible light irradiation (λ ≥ 420 nm) (Fig. 7). The blank tests without catalyst or with catalyst under dark only give trace amount of hydrogen generation. The photocatalytic activity increases gradually with the increase of the molar ratio of Pd in catalysts. The $Ag@Ag_1Pd_1$ alloy catalyst exhibits the highest photocatalytic activity, which is about 26 times higher than the reported hydrogen generation rate from HCHO over Pt/TiO_2 photocatalyst (Table S1) [77,78]. Further increase of Pd loading amount in catalyst leads to decrease of activity for hydrogen evolution, indicating catalytic activity can be optimized by tuning alloy component in catalyst.

Fig. 8 presents the effect of NaOH concentration on photocatalytic activity over $Ag@Ag_1Pd_1$ for hydrogen generation. The best photocatalytic activity was obtained when NaOH concentration was 1 mol/L. It is known that the carboxyl groups of EY will deprotonate in the strongly basic condition, which is beneficial for dye molecule adsorption on catalyst. However, over concentrated NaOH will result in stronger electrostatic repulsion between deprotonated EY and negative catalyst surface, making dye molecule harder adsorb on alloy catalyst. In addition, over concentrated NaOH will also lead to side Cannizzaro reaction, which will also lower hydrogen evolution rate.

Fig. 9 shows the HCHO concentration effects on the hydrogen evolution under visible light irradiation (λ ≥ 420 nm). With the increase of the concentration of HCHO, the hydrogen evolution rates increased first and then decreased. The optimized concentration of HCHO was 0.75 mol/L. Similarly, over concentrated HCHO will also result in the side Cannizzaro reaction and low hydrogen evolution rate.

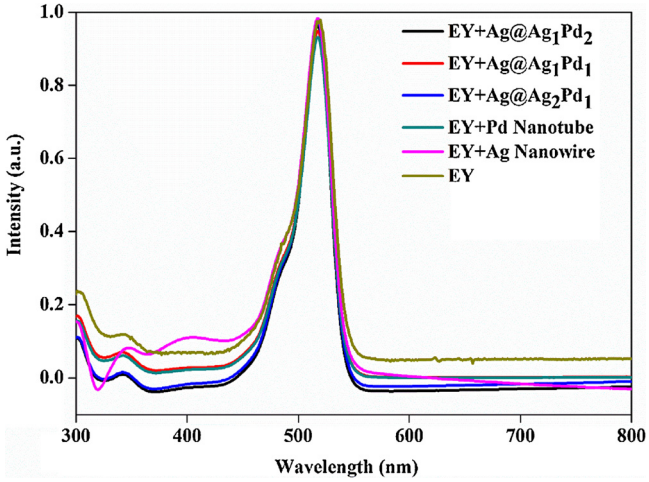

Fig. 6. UV–vis absorption spectra of EY, EY photosensitized Ag nanowire, Pd nanotube, $Ag@Ag_1Pd_2$, $Ag@Ag_1Pd_1$ and $Ag@Ag_2Pd_1$ catalysts.

3.6. Catalyst stability tests

The long-term stability of catalysts was also studied over $Ag@Ag_1Pd_1$ catalyst under visible light irradiation (λ ≥ 420 nm) (shown in Fig. 10). The $Ag@Ag_1Pd_1$ catalyst showed excellent stability for photocatalytic hydrogen evolution from HCHO. In the first run, the

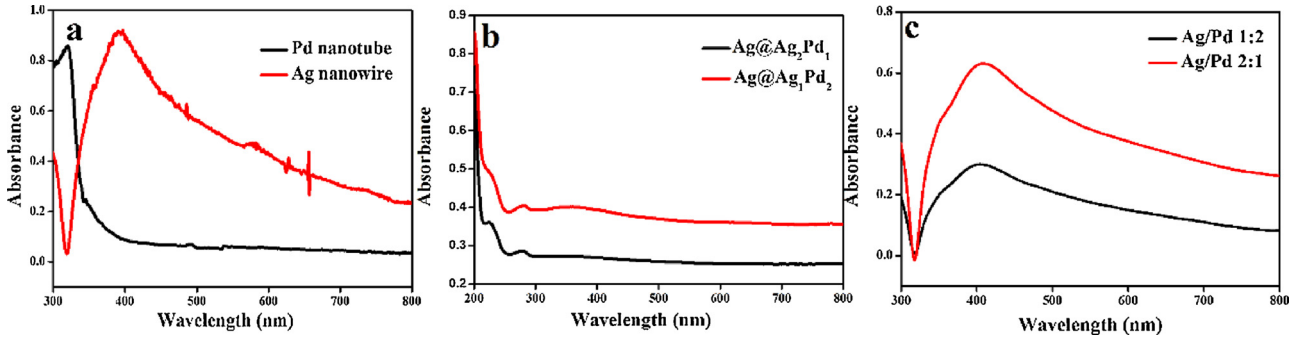

Fig. 5. UV–vis absorption spectra of the different catalysts (a) Ag nanowire and Pd nanotube; (b) Ag-Pd alloy with different composition; (c) physical mixture of Ag and Pd with various ratios.

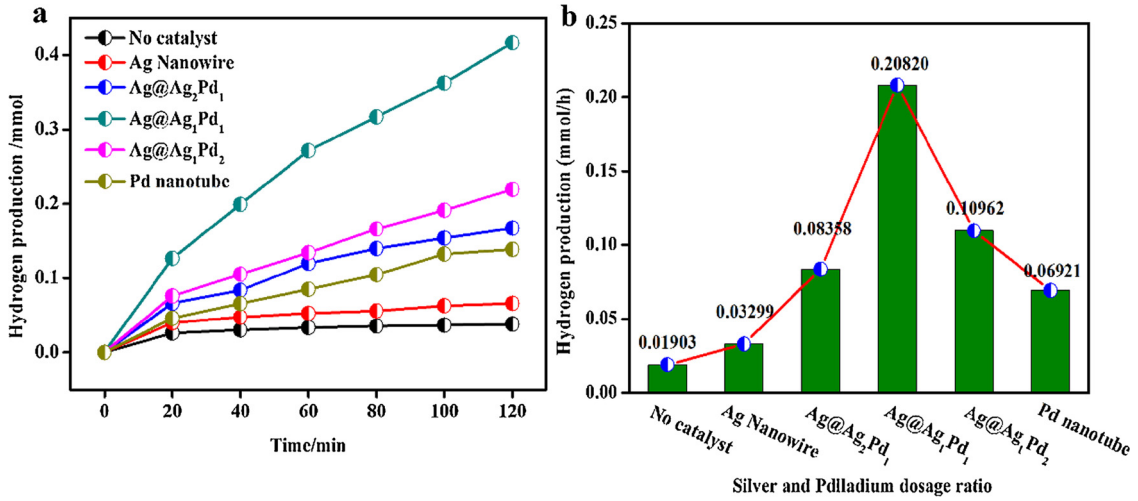

Fig. 7. (a) Photocatalytic activities for hydrogen evolution over Ag nanowire, Pd nanotube, $Ag@Ag_2Pd_1$, $Ag@Ag_1Pd_1$ and $Ag@Ag_1Pd_2$ catalysts under visible light irradiation (≥420 m), (b) The amount of hydrogen produced per hour over different catalysts. Reaction condition: HCHO concentration 0.75 mol/L; NaOH concentration 1.0 mol/L, Catalyst: 5 mg, EY: 35 mg.

hydrogen evolution rate was 41.64 μmol·mg^{-1}·h^{-1}. In the second run, the hydrogen evolution rate was 38.48 μmol·mg^{-1}·h^{-1}. The H_2 evolution activity of the $Ag@Ag_1Pd_1$ catalyst revived to more than 92% of initial activity in the second round. The weak decay of activity in the following cycle tests might due to the catalyst lose during the centrifugation separation of reaction mixture [77,79]. We weighted the remained catalyst after four cycles and found 0.6 mg catalyst lost. In the fifth run, we added 0.6 mg catalyst into reactor and the hydrogen production activity was restored to its original level.

3.7. Isotope experiments

The gas products were identified by the GC–MS. As seen from Fig. 11a, the signals of 2, 32, 40 and 44 *m/z* corresponded to H_2, O_2, Ar and CO_2 detected in the water dispersion. Correspondingly, the isotope tracer experiments presented 3 and 4 *m/z* in D_2O dispersion (shown in Fig. 11b), the *m/z* signals of 3 and 4 correspond to the DH and D_2. That isotope experiments prove that H_2 generates from water and formaldehyde.

It is reasonable to suppose hydrogen generation from formaldehyde over sensitized $Ag@Ag_1Pd_1$ photocatalyst taking placing *via* the following way. Under visible light irradiation, EY absorbs input photons to form singlet excited state EY^{1*}, and then produces the lowest-lying triplet excited state EY^{3*} *via* an intersystem crossing. The excited electron in EY^{3*} can be used to reduce proton to generate hydrogen, while excited dye molecule is quenched by HCHO. Then the dye molecule can absorb next input photon to initiate new cycle of photo-energy conversion.

Such hydrogen evolution process can be studied by photoelectrochemical method. In order to compare the charge formation and transfer over Ag nanowire, Pd nanotube, $Ag@Ag_2Pd_1$, $Ag@Ag_1Pd_1$and $Ag@Ag_1Pd_2$ catalysts, several electrodes using those catalysts were prepared and corresponding electrochemical tests were carried out. As the results shown in Fig. 12, transient photocurrents of Ag nanowire, Pd nanotube, $Ag@Ag_2Pd_1$, $Ag@Ag_1Pd_1$ and $Ag@Ag_1Pd_2$ electrodes all present significant on-off characteristics under visible light irradiation. Among all the electrodes, $Ag@Ag_1Pd_1$ electrode shows the highest photocurrent, indicating that the electron transfer over EY sensitized $Ag@Ag_1Pd_1$ catalyst is the fastest among tested catalysts. More evidence for charge formation and transfer can be obtained by fluorescence lifetime measurement. The lifetime of excited charge reflects the charge formation and transfer, the longer of charge lifetime is measured, the better charge transfer process takes place, corresponding to the better photocatalytic properties. As the results shown in Table 1, the average lifetimes of excited charge over sensitized $Ag@Ag_2Pd_1$, $Ag@Ag_1Pd_1$ and $Ag@Ag_1Pd_2$ are 1.191 ns, 1.201 ns and 1.190 ns

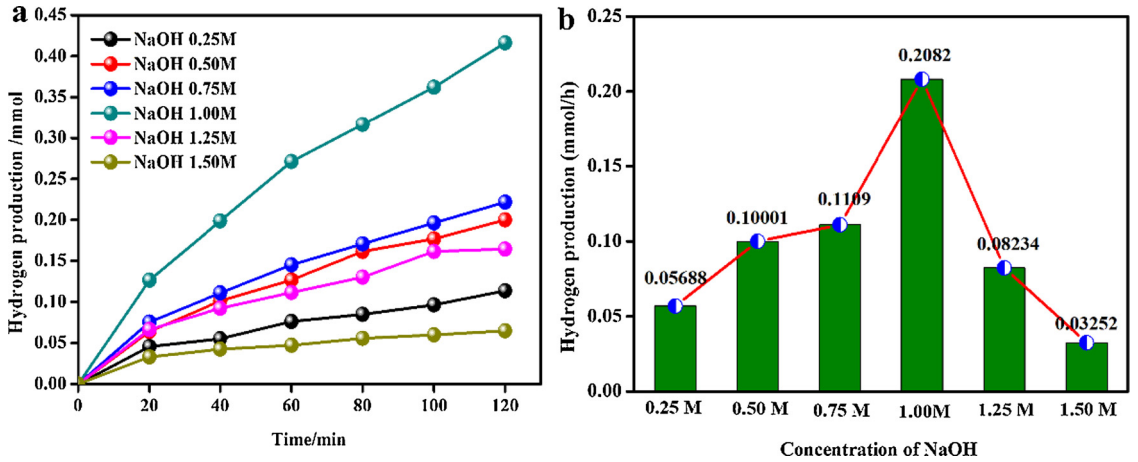

Fig. 8. (a). Effect of NaOH concentrations on hydrogen evolution rate under visible light irradiation, (b). The amount of hydrogen produced from HCHO per hour under different concentration of NaOH. Reaction conditions: HCHO: 0.75 mol/L, catalyst: 5 mg, EY: 35 mg.

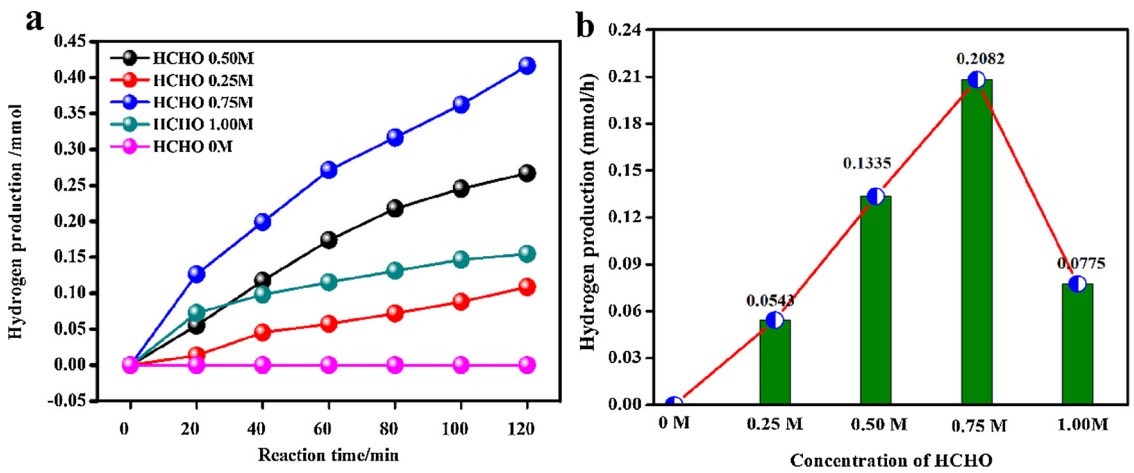

Fig. 9. (a). Effect of HCHO concentrations on hydrogen evolution rate under visible light irradiation (> 420 nm), (b). The amount of hydrogen produced from HCHO per hour under different HCHO concentration. Reaction conditions: NaOH: 1.0 mol/L, catalyst: 5 mg, EY: 35 mg.

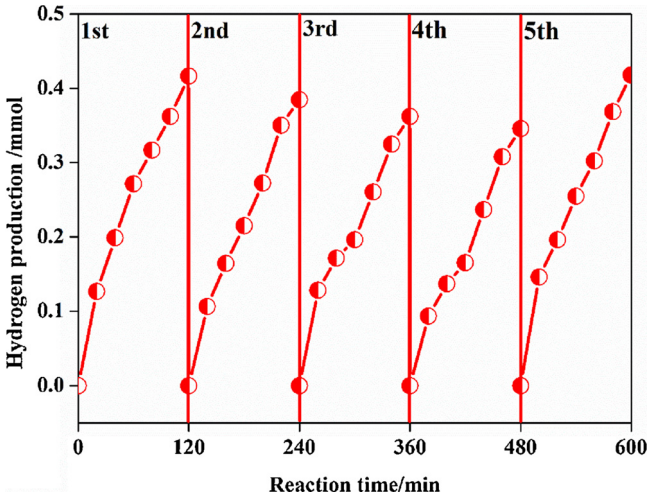

Fig. 10. The cyclic stability tests of hydrogen evolution for $Ag@Ag_1Pd_1$ catalyst under visible light irradiation($\lambda \geq 420$ nm). Reaction Condition: NaOH 1.0 mol/L, HCHO 0.75 mol/L, Catalyst 5 mg, EY 35 mg.

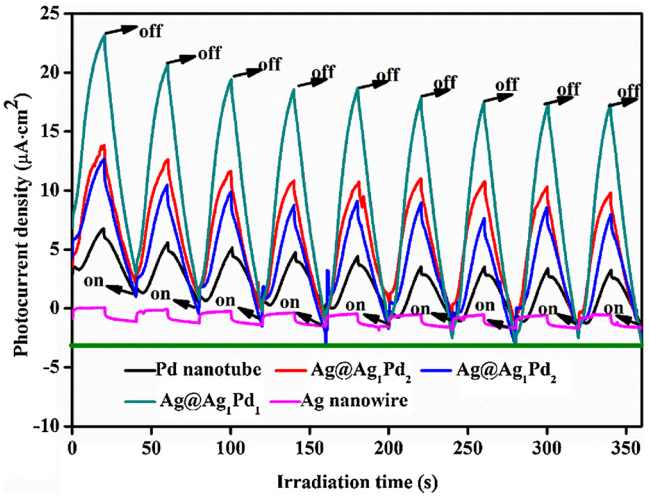

Fig. 12. Transient photocurrent responses over different catalysts.

respectively. $Ag@Ag_1Pd_1$ gives the longest charge lifetime, indicating that the excited charge separation and transfer over $Ag@Ag_1Pd_1$ catalyst is the most efficient among tested catalysts, corresponding to its highest catalytic property for hydrogen generation from formaldehyde.

To study why $Ag@Ag_1Pd_1$ catalyst shows the higher catalytic activity than Ag nanowire and Pd nanotube under visible light irradiation, the adsorption energy of HCHO on catalyst has been calculated according to the models shown in Fig. 13. The calculations are performed by the density functional method with Becke's three parameter exchange function and Lee-Yang-Parr correlation function (B3LYP), and

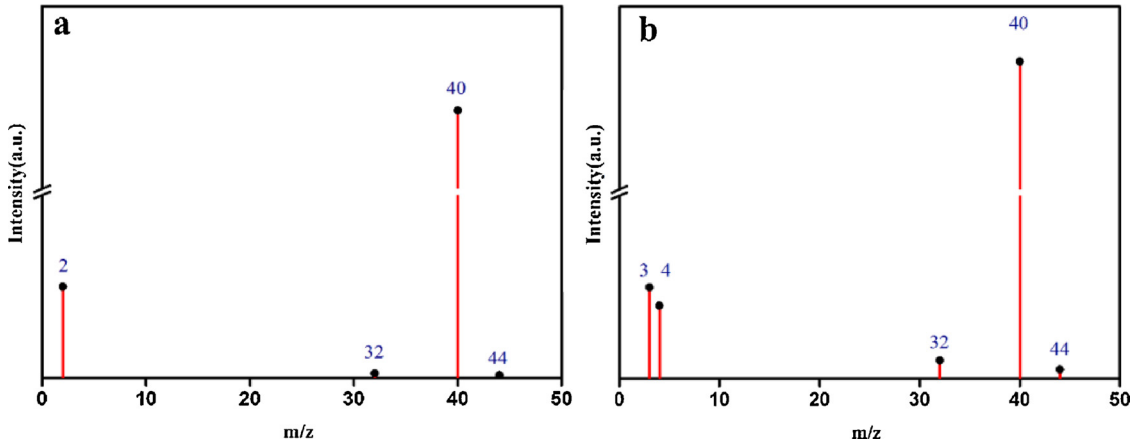

Fig. 11. The gas products detected by GC–MS in photocatalytic hydrogen evolution from formaldehyde over $Ag@Ag_1Pd_1$ catalyst under visible light irradiation ($\lambda \geq 420$ nm), (a) in water, (b) in D_2O.

Table 1
Fluorescence lifetimes of different catalyst samples.

System	lifetime (ns)	Pre-exponential factors B	Average lifetime (ns)	χ^2
EY	τ = 1.151	B1 = 1	τ = 1.151	1.05
Ag nanowire	τ_1 = 0.760	B1 = 0.3191,	τ = 1.184	0.998
	τ_2 = 1.30	B2 = 0.6809		
Pd nanotube	τ_1 = 0.886	B1 = 0.4829,	τ = 1.188	0.995
	τ_2 = 1.370	B2 = 0.5171		
Ag@ Ag_2Pd_1	τ_1 = 0.910	B1 = 0.5335,	τ = 1.191	0.996
	τ_2 = 1.400	B2 = 0.4665		
Ag@ Ag_1Pd_1	τ_1 = 0.786	B1 = 0.6361,	τ = 1.201	1.00
	τ_2 = 1.340	B2 = 0.3639		
Ag@ Ag_1Pd_2	τ_1 = 1.01	B1 = 0.8340,	τ = 1.190	0.996
	τ_2 = 1.72	B2 = 0.1660		

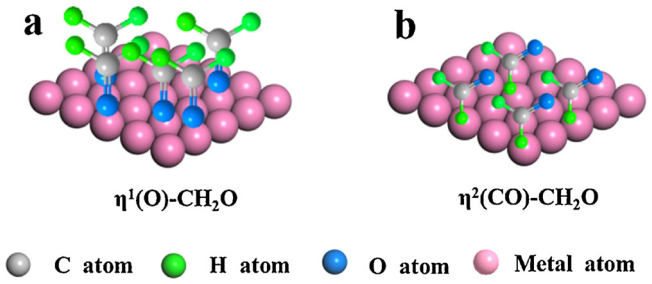

Fig. 13. Adsorption configurations of HCHO on metal surface: (a) η^1(O)-HCHO and (b) η^2(CO)-HCHO.

the basis sets LANL2DZ are employed using Gaussian 03. It is known the absorption configuration of HCHO on different metal surface is dependent on the metal characteristics. On Ag surface, HCHO molecule adsorbs in an η^1-configuration, in which only the oxygen atom interacts with the metal (see Fig. 13a) [80]. In contrast, HCHO adsorbs in an η^2-configuration on Pd and the Ag-Pd alloy surface, in which the carbonyl group is parallel to the surface, and both the C and O atoms interacts with the metal (see Fig. 13b) [81,82].

The adsorption energy (E) is calculated according to equation below,

$$E = E_{ad/sub} - E_{ad} - E_{sub}$$

Where $E_{ad/sub}$ is the total energy of the slab model, and E_{ad} and E_{sub} are the total energies of the formaldehyde in the gas phase, respectively.

According to the calculation results presented in Tables 2 and 3 and Fig. 14, the adsorption energy of η^1-HCHO on Ag surfaces is -4.91 kcal/mol, while the corresponding data are -6.12, -12.5, -20.71 and -21.34 kcal/mol on Ag_2Pd_1, Ag_1Pd_1, Ag_1Pd_2 and pure Pd surface, respectively (see Table 2). The results indicate that the increase of the Pd ratio in the Ag-Pd catalyst leads to the increase of the absorption energy of formaldehyde. Since the better catalytic activity for hydrogen generation from HCHO solution needs the higher adsorption energy [82–85], Pd catalyst shows higher activity than Ag catalyst for formaldehyde conversion to hydrogen. However, the hydrogen formation reaction from formaldehyde is also dependent on the hydrogen

Table 2
The calculated adsorption energies of formaldehyde on different catalysts.

Catalyst	Adsorption energy (kcal/mol)
Ag	**−4.91**
Ag_2Pd_1	**−6.12**
Ag_1Pd_1	**−12.5**
Ag_1Pd_2	**−20.71**
Pd	**−21.34**

Table 3
The calculated adsorption energy of water on different catalyst surface.

Catalyst	Adsorption site	Adsorption energy (kcal/mol)
Ag	Top Ag	−3.34
	Bridge Ag-Ag	−2.49
Ag_2Pd_1	Top Ag	−7.61
	Top Ag	−7.93
Ag_1Pd_1	Top Pd	−16.37
	Bridge Ag-Pd	−14.07
Ag_1Pd_2	Top-Pd	−5.93
Pd	Top-Pd	−4.82

adsorption and desorption on metal catalyst. It is known that hydrogen adsorption energy on Ag (-50.19 kcal/mol) is lower than that on Pd (-62.14 kcal/mol) [56], in addition, the adsorption energy can be tuned in some extent by alloying of Ag and Pd, therefore variation of Ag and Pd ratio can further optimize catalyst performance *via* variation of Pd ratio in catalyst.

We also calculated the adsorption energies of H_2O molecule on different catalysts. The adsorption sites on the (111) surfaces of Ag-Pd alloy are sketched in Fig. 15. Seven kinds of adsorption site are possible on the Ag-Pd (111) surface. However, when the HCHO molecule is adsorbed on the surface of Ag-Pd (111), the available adsorption sites of water molecules will gradually decrease. Fig. 16 shows the possible adsorption H_2O sites on Ag-Pd (111) alloy surface with different Ag-Pd composition. According to the adsorption energies shown in Tables 2 and 3 [85–87], it is reasonable to expect that the water molecule prefer adsorb on the top site on Ag surface, top-Ag site on Ag_2Pd_1, top Pd site on Ag_1Pd_1, top Pd site on Ag_1Pd_2 and top Pd site on Pd. The corresponding adsorption energies are 3.34, -7.61,-16.37,-5.93 and-4.82 kcal/mol. These results indicate that the absorption energy of water increase first and then decrease when the Pd ratio increases in the Ag-Pd alloy. And the Ag_1Pd_1 alloy catalyst shows the highest adsorption energy, correspondingly, these results indicate that Ag@Ag_1Pd_1 catalyst will present the highest photocatalytic activity for hydrogen generation performance.

In Ag-Pd alloy catalyst, orbital overlap Ag and Pd leads to their interaction and d band center shift to the Fermi surface [88,89], which will enhance the interaction between the catalyst and the reactant molecules, thereby increasing the adsorption energy [90–92]. Meanwhile, charges will transfer from Ag to Pd due to their difference of Fermi levels and work functions [93–96]. By variation of metal ratio, tuning of charge density in Ag-Pd alloy catalyst become possible [97], that induces ligand effect on alloy catalysts (see Fig. 17b) and charge re-distribution (see Fig. 17c), which strengthens the adsorption of water molecule through stronger back donation.

At the same time, that charge re-distribution will affect the adsorption energy of HCHO and water on metal catalyst [98,99]. It is known that HCHO molecular mainly adsorbs in a η^1 configuration on Ag (111) surface [100–102], and water molecule absorbs on top site of Ag. However, there is limited available unit on the Ag (111) surface (see Fig. 18a) although the adsorption energy is low. The formaldehyde adsorption configuration is η^2 configuration over Pd surface while the water molecule adsorbs on top site of Pd. On the Ag-Pd alloy surface, the HCHO adsorption configuration is also η^2 configuration with higher adsorption energy, which makes hydrogen evolution efficient (Fig. 18 b and c). In short, the higher activity of the alloy catalyst is due to the adsorption energy difference between formaldehyde and water molecules. By adjusting the composition of the alloy catalyst, the adsorption energy of formaldehyde and water molecules can also be modulated to enhance the hydrogen production activity.

4. Conclusion

In summary, an efficient alloy catalyst for hydrogen generation from

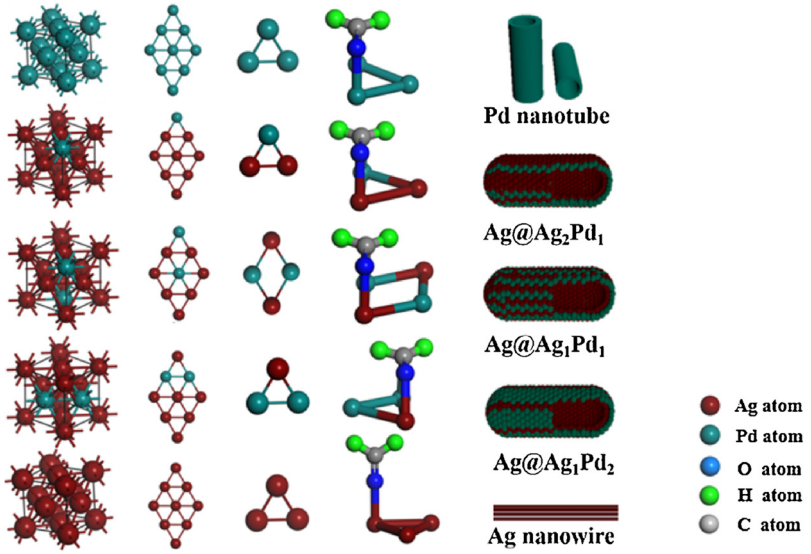

Fig. 14. The adsorption configuration of formaldehyde on different catalyst surface.

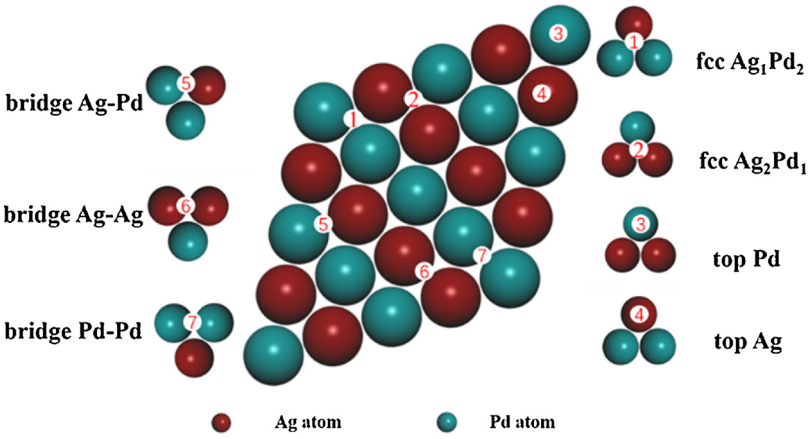

Fig. 15. Top view of adsorption sites on the surfaces (111) Ag-Pd.
Red : Ag; Green: Pd.

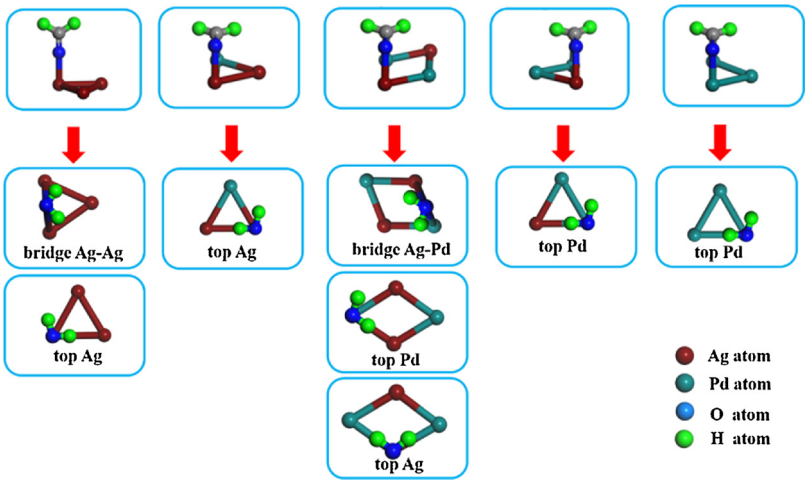

Fig. 16. Top view of all the possible adsorption sites of water molecule on the (111) Ag-Pd surfaces with different composition.

formaldehyde under visible light irradiation has been developed. The as-prepared EY sensitized $Ag@Ag_1Pd_1$ catalyst showed the highest activity for hydrogen evolution. The XRD, XPS, TEM and HRTEM characterizations of as-prepared catalysts indicated the alloy catalysts exhibited core-shell structure with Ag as a core and Ag-Pd alloy as a shell. The adsorption energies of reactant HCHO and water molecules, the ligand effect and surface charge re-distribution on alloy surface determined the activity of alloy catalyst. Moreover, the performance

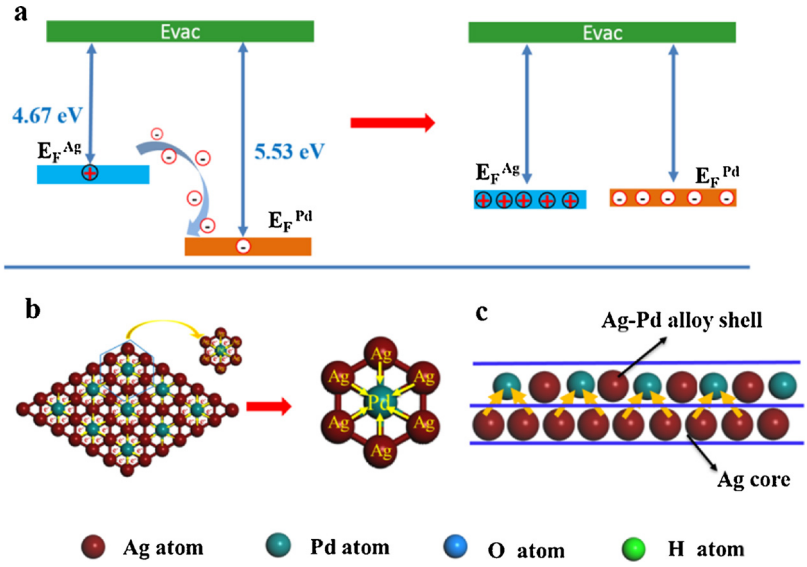

Fig. 17. The schematic of charge re-distribution over alloy catalyst.

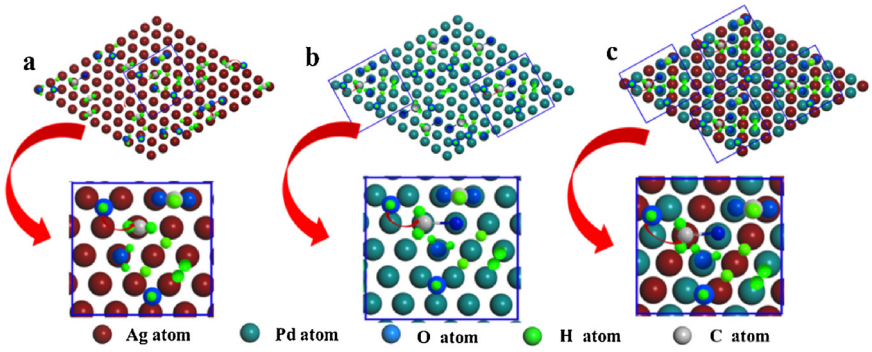

Fig. 18. The photocatalytic hydrogen generation mechanism from HCHO over (a) (111) Ag on Ag nanowire, (b) (111) Pd nanotube, (c) (111) Ag-Pd catalyst.

could be optimized by change of Ag-Pd ratio in alloy catalyst. The preparation regulation of this new alloy catalyst has been verified by density-functional theory (DFT) calculation study, considering adsorption energy over catalyst active sites for formaldehyde and water adsorption, and the hydrogen generation process. The results here can provide a new insight to the cheaper catalyst development for hydrogen generation from formaldehyde driven by visible light irradiation.

Acknowledgements

This work is supported by the National Natural Science Foundation of China (Grant Nos. 21673262 and 21433007), respectively.

Appendix A. Supplementary data

Supplementary material related to this article can be found, in the online version, at doi:https://doi.org/10.1016/j.apcatb.2018.06.028.

References

[1] W. Zhang, C. Kong, G. Lu, Chem. Comm. 51 (2015) 10158–10161.
[2] W.P. Wang, G.X. Lu, Prog. Chem. 15 (2003) 74–78.
[3] P. Liu, J.C. Lu, D.K. Chen, F. Liu, J.P. Liu, J. Yu, K.Z. Chen, Y.M. Luo, J. Mol. Catal. (China) 30 (2016) 480–495.
[4] P. He, Y. Chen, W.F. Fu, J. Mol. Catal. (China) 30 (2016) 269–275.
[5] X.Q. Zhang, D. Luo, W.Y. Zhang, W. Gao, X.F. Ning, H.X. Liu, B. Tian, B.J. Yang, G.X. Lu, Appl. Catal. B 232 (2018) 371–383.
[6] G.X. Lu, W.L. Zhen, J. Mol. Catal. (China) 31 (2017) 299–304.
[7] B. Tian, Z. Li, W. Zhen, G. Lu, J. Phys. Chem. C 120 (2016) 6409–6415.
[8] Q. Li, C.L. Li, F. Wang, Q.J. Ren, Z. Ren, J. Mol. Catal. (China) 30 (2016) 557–565.
[9] Q.L. Zhou, L. Li, C.L. Yang, Y.Z. Jiao, X.Y. Zhang, J. Mol. Catal. (China) 31 (2017) 236–246.
[10] X.F. Ning, W.L. Zhen, Y.Q. Wu, G.X. Lu, Appl. Catal. B 226 (2018) 373–383.
[11] G.X. Lu, W.L. Zhen, J. Mol. Catal. (China) 31 (2017) 299–304.
[12] G.X. Lu, W.L. Zhen, J. Mol. Catal. (China) 31 (2017) 299–304.
[13] S. Ahmed, M. Krumpelt, Int. J. Hydrogen Energy 26 (2001) 291–301.
[14] G.X. Lu, W.Y. Zhang, J. Mol. Catal. (China) 31 (2017) 401–410.
[15] Z.X. Huang, F. Li, Y.X. Li, S.Q. Peng, J. Mol. Catal. (China) 31 (2017) 181–187.
[16] W. Gao, W.Y. Zhang, B. Tian, W.L. Zhen, Y.Q. Wu, X.Q. Zhang, G.X. Lu, Appl. Catal. B 224 (2018) 553–562.
[17] G.X. Lu, B. Tian, J. Mol. Catal. (China) 31 (2017) 101–104.
[18] M. Cargnello, A. Gasparotto, V. Gombac, T. Montini, D. Barreca, P. Fornasiero, Eur. J. Inorg. Chem. (2011) (2011) 4309–4323.
[19] W.L. Zhen, X.F. Ning, B.J. Yang, Y.Q. Wu, Z. Li, G.X. Lu, Appl. Catal. B 221 (2018) 243–257.
[20] Z. Li, B. Tian, W.L. Zhen, W.Y. Zhang, X.Q. Zhang, Y.Q. Wu, G.X. Lu, Appl. Catal. B 219 (2018) 501–510.
[21] W. Gao, W.Y. Zhang, G.X. Lu, Appl. Catal. B 212 (2017) 23–31.
[22] X.F. Ning, J. Li, B. Jang, W.L. Zhen, Z. Li, B. Tian, G.X. Lu, Appl. Catal. B 212 (2017) 129–139.
[23] H.B. Gao, W.L. Zhen, J.T. Ma, G.X. Lu, Appl. Catal. B 206 (2017) 353–363.
[24] M. Wang, Z. Li, Y. Wu, J. Ma, G. Lu, J. Catal. 353 (2017) 162–170.
[25] W.Y. Zhang, G.X. Lu, Catal. Sci. Technol. 6 (2016) 7693–7697.
[26] C. Kong, S.X. Min, G.X. Lu, Chem. Commun. 50 (2014) 9281–9283.
[27] W.Y. Zhang, C. Kong, G.X. Lu, Chem. Commun. 51 (2015) 10158–10161.
[28] W.Y. Zhang, C. Kong, W. Gao, G.X. Lu, Chem. Commun. 52 (2016) 3038–3041.
[29] W.Y. Zhang, W. Gao, X.Q. Zhang, Z. Li, G.X. Lu, Appl. Surf. Sci. 434 (2018) 643–668.
[30] W.Y. Zhang, S.L. Yang, J. Li, W. Gao, Y.B. Deng, W.P. Dong, C.J. Zhao, G.X. Lu, Appl. Catal. B 206 (2017) 89–103.
[31] B. Tian, W. Gao, X. Zhang, Y. Wu, G. Lu, Appl. Catal. B: Environ. 221 (2008) 618–625.
[32] Z. Li, B. Tian, W.Y. Zhang, X.Q. Zhang, Y.Q. Wu, G.X. Lu, Appl. Catal. B 204 (2017) 33–42.
[33] B. Tian, W.L. Zhen, H.B. Gao, X.Q. Zhang, Z. Li, G.X. Lu, Appl. Catal. B 203 (2017) 789–797.

[34] Z. Li, B. Tian, W.L. Zhen, Y.Q. Wu, G.X. Lu, Appl. Catal. B 203 (2017) 408–415.
[35] W.L. Zhen, J.T. Ma, G.X. Lu, Appl. Catal. B 190 (2016) 12–25.
[36] Z. Li, Y.Q. Wu, G.X. Lu, Appl. Catal. B 188 (2016) 56–64.
[37] S. Li, H. Hu, Y. Bi, J. Mater. Chem. A 4 (2016) 796–800.
[38] S. Kapoor, F.A. Barnabas, M.C. Sauer Jr, D. Meisel, C.D. Jonah, J. Phys. Chem. 99 (1995) 6857–6863.
[39] A. Costine, J.S.C. Loh, G. Power, M. Schibeci, R.G. Mcdonald, Ind. Eng. Chem. Res. 50 (2011) 12324–12333.
[40] E.C. Ashby, F. Doctorovich, C.L. Liotta, H.M. Neumann, E.K. Barefield, A. Konda, K. Zhang, J. Hurley, D.D. Siemer, J. Am. Chem. Soc. 115 (1993) 1171–1173.
[41] W.K. Wilmarth, J.C. Dayton, J.M. Flournoy, J. Am. Chem. Soc. 75 (1953) 4549–4553.
[42] J.M. Flournoy, W.K. Wilmarth, J. Am. Chem. Soc. 83 (1961) 2257–2262.
[43] F. Guzman, S.S.C. Steven, C. Yang, Ind. Eng. Chem. Res. 52 (2012) 61–65.
[44] Y. Bi, G. Lu, Nanotech 19 (2008) 275–306.
[45] Y. Bi, G. Lu, Chem. Lett. 37 (2008) 514–515.
[46] Y. Li, G. Lu, S. Li, Chemosphere 52 (2003) 843–850.
[47] M.G. Walter, E.L. Warren, J.R. Mckone, S.W. Boettcher, Q. Mi, E.A. Santori, N.S. Lewis, Chem. Rev. 110 (2010) 6446–6473.
[48] H. Yan, J. Yang, G. Ma, G. Wu, X. Zong, Z. Lei, J. Shi, C. Li, J. Catal. 226 (2009) 165–168.
[49] H. Chen, S. He, X. Cao, S. Zhang, M. Xu, M. Pu, D. Su, M. Wei, D.G. Evans, X. Duan, Chem. Mater. 28 (2016) 4751–4761.
[50] T. Mattila, A. Zunger, J. Appl. Phys. 85 (1999) 160–167.
[51] J. He, T. Kunitake, A. Nakao, Chem. Mater. 15 (2003) 4401–4406.
[52] S. Mukerjee, S. Srinivasan, J. Electro, Chem. Soc. 357 (1993) 201–224.
[53] C.G. Swain, A.L. Powell, W.A. Sheppard, C.R. Morgan, J. Am. Chem. Soc. 101 (1979) 3576–3583.
[54] T. Toda, H. Igarashi, H. Uchida, M. Watanabe, J. Electro. Chem. Soc. 146 (1999) 3750–3756.
[55] S.T. Nguyen, H.M. Law, H.T. Nguyen, N. Kristian, S. Wang, S.H. Chan, X. Wang, Appl. Catal. B 91 (2009) 507–515.
[56] P.A. Sheth, M. Neurock, C.M. Smith, J. Phys. Chem. B. 109 (2005) 12449–12466.
[57] W. Yu, M.D. Porosoff, J.G.G. Chen, Chem. Rev. 112 (2012) 5780–5817.
[58] N.A. Khan, A. Uhl, S. Shaikhutdinov, H.J. Freund, Surf. Sci. 600 (2006) 1849–1853.
[59] E.H. Voogt, A.J.M. Mens, O.L.J. Gijzeman, J.W. Geus, Surf. Sci. 373 (1997) 210–220.
[60] S. González, K.M. Neyman, S. Shaikhutdinov, J. Phys. Chem. C. 111 (2007) 6852–6856.
[61] Y. Liu, G. She, X. Qi, L. Mu, X. Wang, W. Shi, J. Nanosci. Nanotech. 15 (2015) 7068–7073.
[62] N. Mottaghi, M. Ranjbar, H. Farrokhpour, M. Khoshouei, A. Khoshouei, P. Kameli, H. Salamati, M. Tabrizchi, M. Jalilian-Nosrati, Appl. Surf. Sci. 292 (2014) 892–897.
[63] H. Hu, Z. Jiao, J. Ye, G. Lu, Y. Bi, Nano Energy 8 (2014) 103–109.
[64] A.M. Venezia, L.F. Liotta, G. Deganello, Z. Schay, D. Horváth, L. Guczi, Appl. Catal. A 211 (2001) 167–174.
[65] Q. Hu, X. Liu, G. Wang, Chem. Eur. J. 23 (2017) 17659–17662.
[66] D.A. Slanac, W.G. Hardin, K.P. Johnston, J. Am. Chem. Soc. 134 (2012) 9812–9819.
[67] I. Lopez-Salido, D.C. Lim, Y.D. Kim, Sur. Sci. 588 (2005) 6–18.
[68] J. Huang, S. Vongehr, S. Tang, H. Lu, X. Meng, J. Phys. Chem. C 114 (2010) 15005–15010.
[69] A.M. Venezia, L.F. Liotta, G. Deganello, Z. Schay, L. Guczi, J. Catal. 182 (1999) 449–455.
[70] G.B. Hoflund, H.A.E. Hagelin, J.F. Weaver, G.N. Salaita, Appl. Sur. Sci. 2005 (2003) 102–112.
[71] C. Lee, H. Chiou, C. Syu, C. Liu, C. Yang, C. Syu, Int. J. Hydrogen Energy 36 (2011) 12706–12714.
[72] W. Luo, X. Gao, S. Chou, J. Wang, H. Liu, Adv. Mater. 27 (2015) 6862–6869.
[73] L. Chen, W. Zhao, Y. Jiao, Spectrochim. Acta A 68 (2007) 484–490.
[74] Y. Chung, H. Rhee, J. Colloid Int. Sci. 271 (2004) 131–135.
[75] C. Yang, C. Wan, Y. Wang, J. Colloid Int. Sci. 275 (2004) 433–439.
[76] W. Wang, G. Cao, J. Nanopart. Res. 9 (2007) 1153–1161.
[77] P. Chowdhury, G. Malekshoar, M.B. Ray, J. Zhu, A.K. Ray, Ind. Eng. Chem. Res. 52 (2013) 5023–5029.
[78] W. Zhang, C. Kong, W. Gao, G. Lu, Chem. Commun. 52 (2016) 3038–3041.
[79] X. Ning, J. Li, B. Yang, W. Zhen, Z. Li, B. Tian, G. Lu, Appl. Catal. B 212 (2017) 129–139.
[80] L.E. Fleck, Z.C. Ying, M. Feehery, H.L. Dai, Surf. Sci. 296 (1993) 400–409.
[81] E. Jeroro, J.M. Vohs, J. Am. Chem. Soc. 130 (2008) 10199–10207.
[82] A. Sharifi, M.M. Mojtahedi, M.R. Saidi, Tetrahedron Lett. 40 (1999) 1179–1180.
[83] T. Bligaard, J.K. Nørskov, S. Dahl, J. Matthiesen, C.H. Christensen, J. Sehested, J. Catal. 224 (2004) 206–217.
[84] J.B. Miller, B.D. Morreale, A.J. Gellman, Surf. Sci. 202 (2008) 1819–1825.
[85] N.C. Burtch, H. Jasuja, K.S. Walton, Chem. Rev. 114 (2014) 10575–10612.
[86] S. Holloway, K.H. Bennemann, Surf. Sci. 101 (1980) 327–333.
[87] D.R. Alfonso, A.V. Cugini, D.S. Sholl, Surf. Sci. 254 (2003) 12–26.
[88] B. Hammer, J.K. Nørskov, Adv. Catal. 45 (2000) 71–129.
[89] J.K. Nørskov, Rep. Prog. Phy. 53 (1990) 1253–1295.
[90] J.K. Nørskov, Prog. Surf. Sci. 38 (1991) 103–144.
[91] L. Xu, F. Yao, J. Luo, C. Wan, M. Ye, P. Cui, Y. An, RSC Adv. 7 (2017) 4746–4752.
[92] P.B. Balbuena, D. Altomare, A.L. Agapito, J.M. Seminario, J. Phys. Chem. B 07 (2003) 13671–13680.
[93] J. Greeley, M. Mavrikakis, *Nat. Mater.* 3 (2004) 810–815.
[94] K. Tedsree, T. Li, S. Jones, C.W.A. Chan, K.M.K. Yu, P.A.J. Bagot, E.A. Marquis, G.D.W. Smith, S.C.E. Tsang, Nat. Nanotech. 6 (2011) 302–307.
[95] Y. Cao, Z.X. Chen, Surf. Sci. 600 (2008) 4572–4583.
[96] M. Ojeda, E. Iglesia, Angew. Chem. Int. Ed. 48 (2009) 4800–4803.
[97] A.M. Lossack, D.M. Bartels, E. Roduner, Res. Chem. Intermed. 27 (2001) 475–483.
[98] K.H. Lim, Z.X. Chen, K.M. Neyman, N. Rösch, J. Phys. Chem. B 110 (2006) 14890–14897.
[99] H. Kobayashi, M. Yamauchi, H. Kitagawa, Y. Kubota, K. Kato, M. Takata, J. Am. Chem. Soc. 130 (2008) 1828–1829.
[100] D.B. Kokh, R.J. Buenker, H.P. Liebermann, L. Pichl, J.L. Whitten, J. Phys. Chem. B 109 (2005) 18070–18080.
[101] K.T. Chuang, B. Zhou, S. Tong, Ind. Eng. Chem. Res. 33 (1994) 1680–1686.
[102] K. Zhang, R.P. Lively, J.D. Noel, Langmuir 28 (2012) 8664–8673.